Observation of faster-than-diffusion magnetic field penetration into a plasma

R. Arad,[a] K. Tsigutkin, and Y. Maron
Faculty of Physics, Weizmann Institute of Science, Rehovot 76100, Israel

A. Fruchtman
Holon Academic Institute of Technology, Holon 58102, Israel

J. D. Huba
Plasma Physics Division, Naval Research Laboratory, Washington, D.C. 20375

(Received 24 June 2002; accepted 15 October 2002)

Spatially and temporally resolved spectroscopic measurements of the magnetic field, electron density, and turbulent electric fields are used to study the interaction between a pulsed magnetic field and a plasma. In the configuration studied (known as a plasma opening switch) a 150 kA current of 400 ns-duration is conducted through a plasma that fills the region between two planar electrodes. The time-dependent magnetic field, determined from Zeeman splitting, is mapped in three dimensions, showing that the magnetic field propagation is faster than expected from diffusion based on the Spitzer resistivity. Moreover, the measured magnetic field profile and the amplitude of turbulent electric fields indicate that the fast penetration of the magnetic field cannot be explained by an anomalously high resistivity. On the other hand, the magnetic field is found to penetrate into the plasma at a velocity that is independent of the current-generator polarity, contradictory to the predictions of the Hall-field theory. A possible mechanism, independent of the current-generator polarity, based on the formation of small-scale density fluctuations that lead to field penetration via the Hall mechanism, is presented. It is suggested that these density fluctuations may result from the effect of the unmagnetized Rayleigh–Taylor instability on the proton plasma that undergoes a large acceleration under the influence of the magnetic field pressure. © *2003 American Institute of Physics.* [DOI: 10.1063/1.1527630]

I. INTRODUCTION

Rapid magnetic field penetration into collisionless (or nearly collisionless) plasmas and anomalous plasma transport across magnetic fields is a topic that spans various areas of plasma physics and astrophysics. In laboratory plasmas it is demonstrated in magnetic fusion devices,[1] theta pinches,[2,3] ion diodes,[4] plasma switches,[5] and in plasma–beam transport across magnetic fields.[6] In space and astrophysics, plasma transport across magnetic fields is studied in relation to the interaction of the solar wind with the earth's magnetic field,[7] the evolution of solar flares,[8] the coronal heating,[9] and in accretion discs.[10]

Due to the low plasma collisionality, the magnetic field dynamics in such phenomena are not dominated by classical diffusion. For some configurations it has been suggested[11,12] that the rapid field penetration into the plasma results from an instability-induced anomalous collisionality. For another configuration (a reversed-field theta pinch) an explanation based on magnetic tearing and reconnection has been suggested,[13] while in yet another configuration rapid magnetic field penetration due to the Hall field has been demonstrated.[14]

The evolution of a magnetic field in a plasma, derived from Faraday's law, generalized Ohm's law with the neglect of the electron inertia, and Ampère's law with neglect of the displacement current can be expressed by

$$\frac{\partial \vec{B}}{\partial t} = \vec{\nabla} \times (\vec{v}_i \times \vec{B}) - \vec{\nabla} \times \left(\frac{\vec{j} \times \vec{B}}{e n_e} \right) + \frac{\eta}{\mu_0} \nabla^2 \vec{B}, \tag{1}$$

where the first term on the right hand side is the convection term, the second is the Hall term and the third is the diffusion term. Here, $\vec{v}_i$ is the ion velocity, n_e is the electron density, e is the electron charge, $\vec{j}$ is the current density, $\vec{B}$ is the magnetic field, η is the resistivity, and μ_0 is the permeability of free space.

If the Hall and diffusion terms are neglected (likely to occur in relatively dense and/or uniform plasmas and in low resistivity plasmas) the magnetic field is frozen into the ion fluid. In this case the dominant process is expected to be plasma pushing by the $\vec{j} \times \vec{B}$ force.[15] This can result in a snowplow[16] (in the high-density limit) or specular reflection[17] (in collisionless plasmas) of the plasma in two extreme cases. When the Hall field dominates, the field may penetrate fast as borne out by the treatment based on electron magnetohydrodynamic theory.[18–20] The Hall term is expected to be dominant for scale lengths $L = [d \ln(n)/dx]^{-1}$ that are smaller than the ion inertial length, i.e., $L \ll c/\omega_{pi}$, where ω_{pi} is the ion plasma frequency and c is the speed of light. The characteristic magnetic field penetration velocity into the plasma is then given by[18] $v_H = B/(2\mu_0 e n_e L)$. As

[a]Electronic mail: fnarad@plasma-gate.weizmann.ac.il

demonstrated experimentally,[21] such field penetration results in ion velocities that are lower than the magnetic field velocity and scale linearly as a function of the ion charge-to-mass ratio.

However, for higher electron densities the dominance of the Hall field diminishes and the effects of field penetration and the plasma pushing can be comparable. Moreover, the presence of multi-ion species in the plasma, as is often the case for laboratory plasmas, further complicates the interaction between the plasma and the magnetic field. For instance, we have recently shown in another experiment[22] that species separation in which protons are reflected by the magnetic field and the carbon–ion plasma is penetrated by the magnetic field can occur. Hence, the fluid picture depicted in Eq. (1) should be expanded or reformulated to incorporate phenomena such as species separation that until now have only been addressed theoretically for the highly collisional case.[23]

The present experiment is performed in a configuration referred to as a planar plasma opening switch (POS)[24–27] in which a 150 kA-current is driven through a plasma prefilling the volume between two parallel electrodes. The experiment was designed for studying the magnetic field evolution and ion dynamics for conditions where the magnetic field penetration, expected from treatments based on the Hall effect, is comparable to the characteristic plasma pushing velocity. To this end, the present experiment is designed to have a higher electron density and a longer conduction time in comparison with previous experiments.[14,21,22] Also, the planar geometry eliminates the effect of magnetic field curvature that dominated previous coaxial configurations, thereby decreasing the Hall term.

As has been previously described[28] and will be discussed in more detail,[29] in a multi-ion-species plasma the light-ion plasma may be dominated by pushing while the heavier-ion plasma may be dominated by field penetration. Hence, for investigating the motion of ions of different charges and masses, a plasma consisting of carbon and hydrogen is used.

Detailed investigations of magnetic field–plasma interaction require spatially and temporally resolved measurements of the magnetic field, electron density and ion velocities. In previous studies of similar configurations the magnetic field was obtained from probes,[24,27,30–32] which indicated fast magnetic field penetration into the plasma. Investigations of the plasma dynamics were made by observing the line-integrated electron density, using interferometry,[24,33,34] which demonstrated a drop of this parameter during or after the field penetration.

In the past, magnetic field evolution was also obtained from Zeeman splitting of doped ions.[14] For the present study we developed a plasma doping technique[35] of gaseous elements in order to use line emission from neutral helium for Zeeman splitting. The use of neutral-atom line emission for these measurements avoids the effects of Doppler shifts and broadening found for ions as a result of ion acceleration by the magnetic field. This advantage over our previous work allowed us to improve the accuracy of the magnetic field measurements. Moreover, the use of plasma doping allows for measurements that are spatially resolved in three dimensions (3D), which is essential for unambiguous interpretation of the results. Our measurements allowed for generating a time-dependent 3D map of the magnetic field that can also be used for the understanding of the ion acceleration towards the electrodes. Previous planar geometry experiments[25,36] suggested a peaking of the magnetic field at the electrode edges leading to pinching of the plasma. Here, the magnetic field distribution, measured as a function of the position along the electrode width, showed a uniform current distribution.

The electron density evolution is obtained from the time-dependent population of a low-lying *B* III level (boron doping is described in Sec. II) that is insensitive to variations in the electron energy (the electron energy distribution is studied from high-lying levels of various species[37]). Our measurements yielded the time-dependent magnetic field and electron density in the same plasma region, which demonstrated that the magnetic field penetrates the plasma before the electron density drops. The subsequent electron-density drop is explained[28] by the expulsion of the protons and their co-moving electrons and pushing of the carbon plasma towards the electrodes.

The possibility of increased plasma collisionality due to the growth of current-driven instabilities such as the ion-acoustic and lower-hybrid drift instabilities has been previously discussed.[2,11,38,39] Here, in order to estimate the anomalous plasma collisionality we measured the amplitude and obtained bounds on the frequency of the turbulent electric fields using Stark broadening of hydrogen and helium lines. For these instabilities the amplitude of the turbulent electric fields is found to result in a collisionality that is too small to explain the magnetic field penetration into the carbon plasma by diffusion. In addition, the axial profile of the magnetic field also appears to be inconsistent with magnetic field diffusion.

In order to examine whether in the higher-density, planar configuration the rapid magnetic field penetration into the plasma can be explained by treatments based on the Hall effect, experiments with a reversed-polarity current-generator were performed. These measurements demonstrated that the magnetic field evolution is independent of the current flow direction, in contrast to the theoretical predictions based on the initial electron density gradient across the anode-cathode ($A-K$) gap and the Hall-field model.[18–20] However, it is possible, in principle, that the magnetic field penetration results from the Hall effect near small-scale density fluctuations as previously suggested.[19,40,41] We explore the possibility that such small-scale density fluctuations are indeed generated as a result of the Rayleigh–Taylor instability.[42]

It is well known that in high-current high-voltage plasma systems the determination of the inductance of the device is rather difficult due to the lack of knowledge of the current distribution. Measurements of the magnetic field distribution allow for obtaining the true system inductance, as is demonstrated in the present study.

The energy dissipation associated with the magnetic field penetration has been investigated previously theoretically[43,44] and experimentally[21] with significant discrepancies remaining between theory and observations. If the dominant process

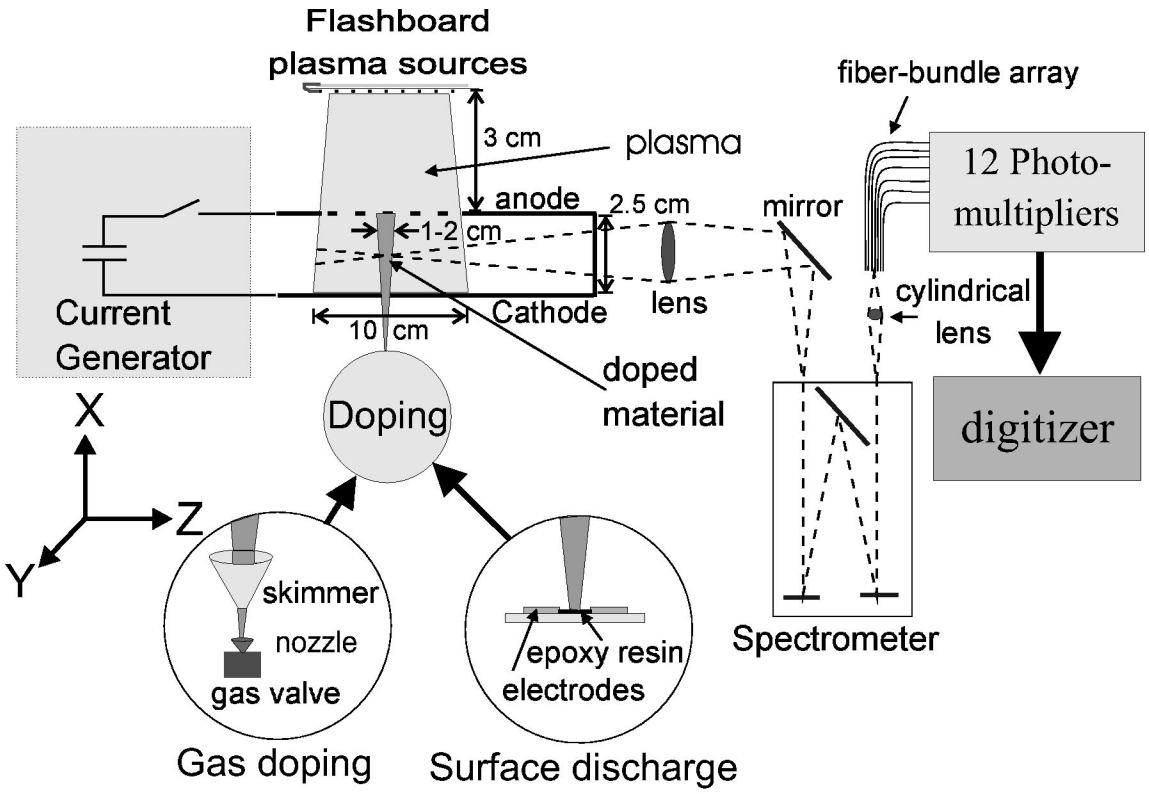

FIG. 1. The experimental system. The inter-electrode region is prefilled with plasma from two flashboard plasma sources. Two techniques are used to locally dope the plasma with various elements. Lenses and mirrors are used to collect light from the doped column into the spectrometer. A cylindrical lens focuses the output of the spectrometer onto a fiber-bundle array that transmits the light to 12 photomultiplier tubes.

is magnetic field penetration and the ions remain immobile,[44] electron heating is expected to result in keV-energy electrons, which have not yet been seen experimentally.[21] Recently, we observed magnetic field penetration that is accompanied by reflection of protons,[22,28] which accounts for a significant fraction of the dissipated energy. In this work, the energy dissipation is predicted from the measured magnetic field profile by time-integrating the Poynting flux at the plasma boundary. It is shown that accounting for the rise-in-time of the magnetic field at the generator and knowledge of the magnetic field spatial distribution leads to a prediction of less energy dissipation, bringing the calculated energy dissipation closer to the observed values. In a future publication,[37] we will present evidence that the mean electron energy is higher than previously reported,[21] which helps to fully elucidate the various channels of the energy dissipation.

II. EXPERIMENTAL SETUP

The experimental setup consists of two planar, 14 cm-wide electrodes separated by a 2.5 cm gap. In the 8 cm-long plasma prefilled region, the electrodes consist of two 5 mm-wide edge strips and 8 0.1 cm-diameter wires with a high geometric transparency of 93%. The following coordinates are defined: $x=0$ is the cathode surface, $y=0$ is the center of the electrodes, and $z=0$ is the generator-side edge of the wire-anode (see Fig. 1 for the orientation of the axes). Throughout this paper the term ''axial'' is used to denote the z direction (towards the load), as analogous to the axial coordinate in coaxial plasma opening switches. At $z=0$, the upstream inductance is 62 ± 4 nH and the downstream inductance that serves as an inductive load is 30 nH.

Two surface-flashover (flashboard) plasma sources, driven by a single 2.8 μF capacitor, charged to 35 kV, are mounted 3 cm above the wire-anode and are operated 1.1 μs prior to the application of the generator current pulse. Each flashboard consists of eight chains with the current through each chain reaching a peak value of 6.5 kA at $t=1.2$ μs. Details of the flashboard-plasma parameters are given in Ref. 46 At $x=1$ cm the plasma consists of protons ($n_p=2\pm1\times10^{14}$ cm^{-3}) and carbon ions ($n_c=1.1\pm0.4\times10^{14}$ cm^{-3}, with a mean charge $+2.7$). The electron density prior to the application of the current pulse was found to vary from $(3\pm0.5)\times10^{14}$ cm^{-3} near the cathode to $(7\pm1)\times10^{14}$ cm^{-3} near the anode and the initial electron temperature was determined to be 6.5 ± 0.5 eV.

In order to perform spatially resolved spectroscopic measurements we dope the plasma with various elements using two doping techniques. The gas doping arrangement,[35] consisting of a fast gas valve, a nozzle, and a skimmer, is mounted below the cathode on a moveable stand that allows for 2D movement. The gas density could be varied from 10^{13} to 10^{15} cm^{-3} and the full width half maximum (FWHM) of the gas beam perpendicular to its injection direction could be varied from 1 to 2 cm.

For doping solid materials we used an electrical discharge over an epoxy resin mixed with the selected element, placed 2 cm below the cathode. The discharge is driven by a

2 μF capacitor charged to 6 kV, yielding a dopant column about 2 cm wide. For the short time delays used in the present experiments, the electron density of the plasma formed by the surface-flashover doping discharge was found to be less than 1×10^{13} cm^{-3} (determined spectroscopically), ensuring no significant effect on the prefilled plasma parameters.

Figure 1 shows a schematic description of the experiment including the plasma sources, the doping arrangements, and the uv-visible spectroscopic system that consists of a 1-meter spectrometer equipped with a 2400 grooves/mm grating. Observations are possible along the x (through the flashboards), y, or the z directions. A cylindrical lens images the light at the output of the spectrometer onto a rectangular fiber-bundle array allowing for observations with different spectral dispersions in the range of 0.07–1 Å/fiber, which also determines the spectral resolution of the system. The spectral dispersion and instrumental broadening were measured using lamps with spectral widths of ≈0.01 Å to an accuracy of 3%. The optical-fiber array consists of 12 fiber columns that transmit the light into 12 photomultipliers (PMTs) yielding a 7 ns temporal resolution. The spatial resolution along the line of sight, determined by the doped-column width, was 1 to 2 cm, whereas the resolutions in the orthogonal directions were set to be 0.1 and 0.4–1 cm, along the x and z directions, respectively. The optical system was absolutely calibrated with an accuracy of $\pm30\%$.

III. EXPERIMENTAL RESULTS

A. Measurements and data analysis

In our measurements, we observed the intensities and spectral profiles of various emission lines from materials doped into the plasma and from the plasma constituents such as hydrogen and carbon. All the observed spectral lines are optically thin, allowing for reliable determination of the absolute upper level populations from the observed line intensities.

All the spectral lines except for those of hydrogen and some lines of neutral helium are dominated by Doppler broadening (Stark and Zeeman splitting are negligible).

The Stark-dominated H_β and He I $4d(^1D)-2p(^1P^0)$ lines are used to study the amplitude of turbulent electric fields in the plasma. The spectral profiles of helium lines used to study the magnetic field are fitted using a number of Gaussians for each of the spectral-line components, where the width of each component is assumed to be due to instrumental and Doppler broadening. The effects of Stark broadening, as a result of electric fields in the plasma, are found to be negligible for the He I $3d(^1D)-2p(^1P^0)$ line, used for the Zeeman splitting measurements.

The measured line intensities are analyzed with the aid of time-dependent collisional-radiative (CR) calculations[46] that determine the level populations as a function of time by solving a series of rate equations for the various atomic processes for given initial particle densities. In these calculations a time-dependent electron density $n_e(t)$ and an arbitrary electron energy distribution are used as input parameters, as described in detail in Ref. 45.

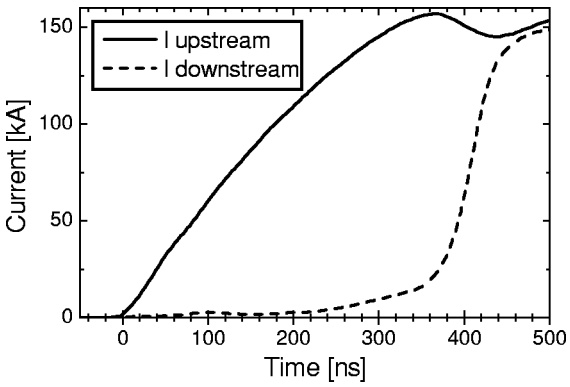

FIG. 2. Traces of the current upstream and downstream of the plasma monitored using two self-integrating Rogowskii coils.

In some measurements the x distribution of the emission intensity of a certain spectral line was studied in a single discharge by opening the spectrometer input slit width to 3 mm. In these measurements the time-dependent intensity of the B III doublet (2065.8 and 2067.2 Å) was observed with a 4.5 mm-resolution across the entire A-K gap.

B. Electrical properties

The currents upstream and downstream of the plasma are monitored using two Rogowskii coils that are calibrated to an accuracy of $\pm7\%$. Typical traces are shown in Fig. 2. The period of current conduction by the plasma, which is the time from the initiation of the upstream current until the sharp rise in the downstream current begins, varies from 360 to 400 ns due to fluctuations in the initial plasma conditions. The time delay between the flashboard and the application of the generator current pulse was varied from 1.05 to 1.15 μs to obtain similiar downstream current characteristics in all the experiments.

C. Magnetic field mapping from Zeeman splitting

The evolution of the magnetic field is determined from the Zeeman splitting of the He I 6678 Å line. The line of sight in these measurements was in the y direction (the direction of the magnetic field), thus only yielding the σ components of the line, split by ±0.021 Å/kG. The helium was doped at $y=0$. The spatial resolutions were 0.1, 2, and 0.5 cm along the x, y, and z directions, respectively and the temporal resolution in these measurements was 16 ns.

Analysis of the line profiles requires knowledge of the line Doppler broadening. To this end, we used the He I 5015 Å line that is insensitive to Zeeman and Stark broadening. The width of this line that is dominated by the instrumental and Doppler broadening was found to remain constant throughout the pulse, indicating, as expected, that the Doppler broadening remains small.

The evolution of the line splitting in time near the generator-side edge of the plasma ($z=-1$ cm) is demonstrated in Figs. 3(a)–3(c). The profile at $t=0$, before the application of the generator current, illustrates the initial line profile. Profiles (b) and (c) show the evolution of the line profile at the same position. The effect of the Zeeman split-

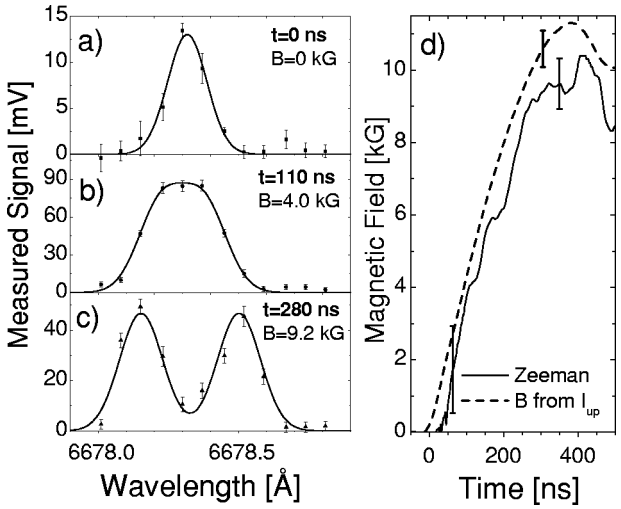

FIG. 3. (a)–(c) Profiles of the He I 6678 Å line fitted by a Gaussian for each of the line components at $t=0$, 110, and 280 ns. (d) The evolution of the magnetic field at the generator-side edge of the plasma 0.5 cm from the cathode in the middle of the electrodes in the y direction. Also shown is the magnetic field deduced from the upstream current assuming uniform current distribution along the y direction.

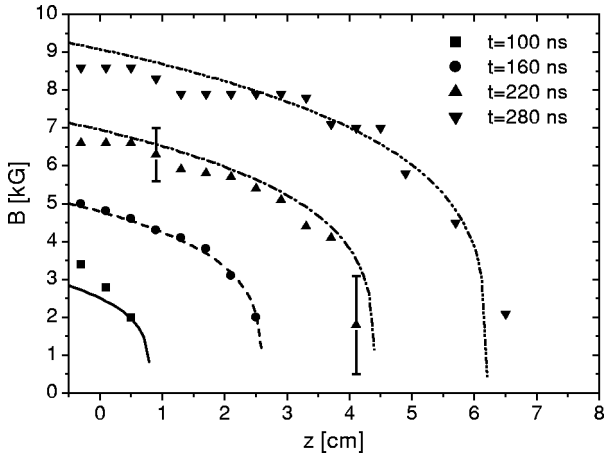

FIG. 4. The magnetic field distribution as a function of the axial position at 1 cm from the cathode surface in the middle of the electrodes in the y direction for various times. The experimental points are fitted by an analytic function [Eq. (2)], with $p=0.25$ and $v=3\times10^7$ cm/s.

ting on the line profile is noticeable at $t=110$ ns, and the splitting is well seen at later times. Note that the widths of each component of the split line is the same as the width prior to the current pulse, consistent with the constant width of the 5015 Å line.

The measured spectra are fitted by constant-width profiles for each of the line components to yield the magnetic field. The accuracy of the magnetic field obtained was found to be ±1.2 kG for $B<4$ kG, when the Zeeman splitting is not resolved, and ±0.7 kG for $B>5$ kG when the two peaks of the pattern are clearly seen. Figure 3 also shows the magnetic field determined from the Zeeman splitting and the one calculated from the upstream current assuming a uniform current distribution along the y direction [demonstrated in Fig. 6(b)]. The magnetic field from the Zeeman splitting is approximately 10% lower possibly due to some current flow between the observation point and the generator. The possible presence of magnetic field components other than B_y has been investigated using polarization-dependent observations, which showed that B_x and $B_z<3$ kG. The total magnetic field may thus be up to 10% larger than the here presented data, i.e., within the indicated uncertainty.

Measurements at different axial positions allow us to construct a 1D map of the magnetic field as a function of the axial position. Figure 4 shows the magnetic-field distribution 1 cm from the cathode and in the middle of the electrode y dimension, at different times. It is instructive to fit the measured data with a simple analytic function. We note that the evolution of the measured magnetic field profile is influenced by the rise-in-time of the generator current $I_G(t)$ and a term that reflects the axial propagation of the magnetic field. To this end, we attempted to fit the measured points using a function of the following form:

$$B(z,t)=B_G(t)\left(1-\frac{z-z_0}{vt}\right)^p, \tag{2}$$

where v is velocity of the magnetic field propagation, z_0 is the position of the vacuum-plasma boundary at the generator side (assumed to be time-independent). $B_G(t)$ is the magnetic field at the generator-side edge of the plasma, approximated by a linear rise in time, $B_G(t)=\mu_0 I_G(t)/a=B_0 t/\tau$, using $\tau=300$ ns, $B_0=10$ kG [according to Fig. 3(d)], and a is the effective electrode dimension along the magnetic field. The value of a has been computed for our electrode geometry [assuming a uniform distribution of the current in ten wires, see Fig. 6(b)] and is found to be 25% larger than the physical width of the electrodes.

The parameter p describes the shape of the magnetic field profile so that when $p\to0$ the axial profile of the magnetic field becomes rectangular while in the limit $p\to1$ it decreases linearly with z. Figure 4 shows that the experimental magnetic field can be fitted reasonably well using $p=0.25$, $z_0=-2.2$ cm, and a constant propagation velocity $v=3\times10^7$ cm/s. Note that the magnetic field has a relatively sharp magnetic field front and a small gradient, resulting from the rise-in-time of the generator current.

In order to obtain a 2D map of the magnetic field, a series of measurements was carried out at $x=0.4$, 1.0, and 2.2 cm, $y=0$, and at $z=-1.0$, -0.3, 1.7, 3.7, 5.7, 7.7, and 9.7 cm. For each position, the magnetic field was averaged over a few discharges and a time-dependent map $B(x,z)$ was constructed using a bilinear extrapolation method. Figure 5 shows the magnetic field maps at $t=120$, 180, 240, and 300 ns. At $t=120$ and 180 ns the front of the magnetic field ($B\leqslant4$ kG) is seen to propagate nearly in a 1D form. At later times, however, the magnetic field structure for $B>4$ kG resembles a wedge shape (similar to the results of Ref. 27). In this figure too, as was shown in Fig. 4 at $x=1$ cm, the width of the current-carrying region is seen to be 2 to 3 cm throughout the pulse, except near the anode at $t>240$ ns, where it is even wider. At $t=300$ ns a region with a low current density is formed at the generator-side edge of the plasma (near the cathode this region extends axially over most of the plasma). The reason for the lack of current flow at this position is probably related to the drop of the electron

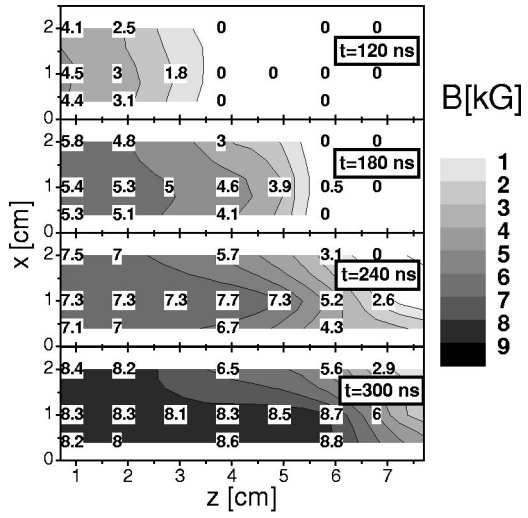

FIG. 5. Four maps of the time-dependent 2D magnetic field distribution. Contours of constant magnetic field are drawn in the xz plane and are shaded according to the color scheme shown on the right. The numbers on the graph represent the measured magnetic field. The spatial resolution in these measurements is 1 cm along the z direction and 0.1 cm along the x direction, and the error of the magnetic field is ± 1.2 kG for $B<4$ kG and ± 0.7 kG for $B>5$ kG.

density in that region, as will be demonstrated in Sec. III E.

To evaluate the asymmetry introduced to the problem by the electrode geometry and the current flow through the plasma, two types of measurements of the magnetic field along the width of the electrodes $B(y)$ were performed.

We first used a $\dot{B}$ loop with no plasma prefilling in order to study the effect of the electrode geometry. Figure 6(a) shows that the magnetic field at the edge of the electrodes increases to 118% of its value in the center of the electrodes, dropping to half its peak value at 1 cm beyond the edge of the electrodes. Figure 6(a) also shows the predicted magnetic field y distribution for a current that is peaked at the edge wires. In this model 82% of the current was uniformly distributed in 10 wires, equally spaced along 13.2 cm, and the remaining current was assumed to flow only in the edge wires. The good fit to the experimental data indicates that indeed, without plasma prefill, 18% of the total generator current passes through the two edge-strips of each of the electrodes. The disagreement at $y=\pm 5.5$ cm results from the somewhat larger wire spacing there that is not accounted for in the model. Note that the ripple in calculated B_y, caused by the relatively large electrode-wire separation, is found to be negligible in the middle of the A-K gap and $\pm 7\%$ at 0.5 cm from either electrode.

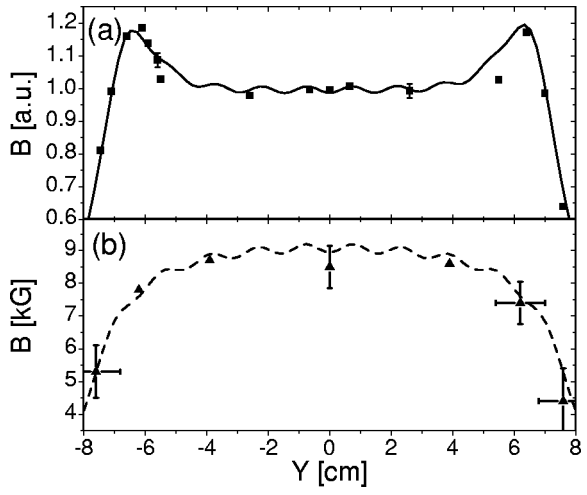

FIG. 6. (a) The magnetic field profile without plasma obtained using a magnetic probe (symbols). Also shown (solid curve) is a calculation in which 82% of the current is uniformly distributed in ten wires and the remaining current flows in the two edge wires. (b) The magnetic field y distribution at $t=300$ ns, $x=1.2$ and $z=1$ cm obtained spectroscopically (symbols), together with a numerical calculations obtained assuming a uniform current distribution over all wires (dashed line).

The magnetic field y distribution was also studied from Zeeman splitting measurements at $z=1$ cm, $x=1.2$ cm, and $y=0$, ± 3.9 cm, ± 6.2, and ± 7.6 cm. Figure 6(b) shows the magnetic field profile at $t=300$ ns together with a numerical calculation. The good fit of the calculated curve, obtained assuming a uniformly distributed current along the equidistant wires, indicates that the nonuniform current distribution shown in Fig. 6(a) becomes approximately uniform during the current conduction by the plasma. Presumably this results from a plasma extent in the y direction that is smaller than the electrode y dimension causing a reduction in the current in the edge electrode strips.

D. The effects of the electrode geometry and polarity

In order to estimate the effects of the electrode wire-geometry on the magnetic field evolution we performed a series of measurements in which the two electrodes, that normally consisted of 1 mm wires spaced 1.3 cm apart, were covered by a mesh. The mesh was made of 50 μm stainless steel wires spaced 0.05 cm apart resulting in a geometric transparency of approximately 80%. The electron density prior to the application of the current pulse was found to be somewhat lower with the mesh. We thus used a longer time delay (≈ 200 ns) between the plasma formation and the application of the current pulse in order to allow for a higher-density plasma to reach the A-K gap. In those experiments it was found that the magnetic field evolution is similar to that with the wire electrodes, indicating that the asymmetry imposed by the wire-electrodes is not responsible for the observed magnetic field evolution.

Measurements with a reversed current-generator polarity, in which the plasma parameters remained unchanged, were performed in order to investigate whether the magnetic field propagation depends on the current flow direction. Figure 7(a) shows the magnetic field evolution at $x=1$ cm in the middle of the plasma y and z dimensions for the two polarities, demonstrating within the experimental reproducibility, the absence of a polarity effect. Furthermore, Fig. 7(b) that shows the populations of the B III $2p$ level, used in Sec. III E for determining the electron density, shows that the time-dependent electron density is also similar for the two polarities. We conclude from this that the magnetic field propagation is independent of the relative directions of the current flow and the electron density gradient in the plasma.

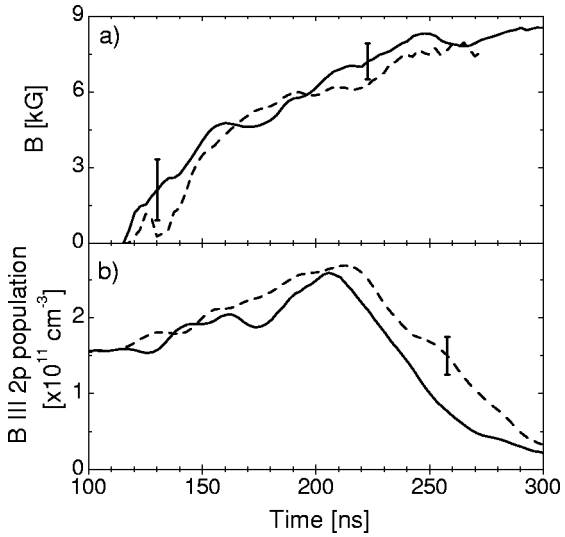

FIG. 7. (a) A comparison between the magnetic field from Zeeman splitting for two polarities at $x=1$, $z=3.7$, and $y=0$ cm. The solid lines refer to experiments with the polarity normally used in this study and the dashed lines to the reversed polarity. (b) A similar comparison of the *B* III $2p$ level population that is used for deducing the electron density.

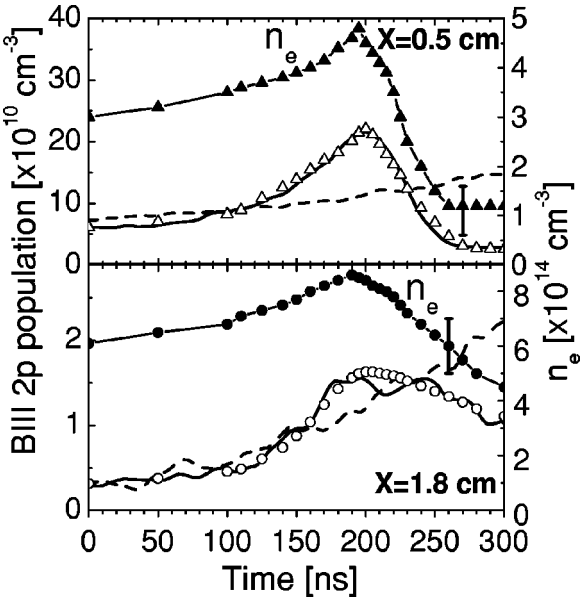

FIG. 8. The evolution of the *B* III $2p$ level as determined from the intensity of the 2066 Å spectral line. The traces are shown for experiments at $x=0.5$ and 1.8 cm, $y=0$, and $z=3.7$ cm with (solid line) and without (dashed) application of the current pulse. The open symbols show CR modeling predictions of the *B* III $2p$ population using the electron density denoted by the full symbols.

E. Time history of the electron density

The electron density distribution prior to the application of the current pulse was obtained from Stark broadening of hydrogen lines.[45] The temporal evolution of the electron density is studied from the line intensity of a *B* III line ($2p-2s$, 2066 Å), where *B* III is injected to the observation region using the surface flashover doping technique.[45] This line intensity is insensitive to the electron temperature within the range considered ($\geqslant 6$ eV, as will be shown in a subsequent publication[37]). Some of the measurements were performed with the "open slit" configuration (described in Sec. III A), allowing for time-dependent observations of the line intensity at 10 positions across the A-K gap in a single discharge, thus eliminating the effects of the experimental irreproducibilities. The spatial resolutions in these measurements are 0.45 and 0.25 cm in the x and z directions, respectively.

In Fig. 8 we present the temporal evolution of the *B* III $2p$ population at two positions across the A–K gap in the middle of the plasma y and z dimensions. It is seen that at both positions the level populations start dropping at $t \approx 200$ ns. For reference, the level populations with only the application of the plasma source are also given, demonstrating the continuous rise of the population in the absence of the generator current pulse.

We now infer the time-dependent electron density $n_e(t)$ from the history of the *B* III level population using our CR modeling to find the $n_e(t)$ that provides the best fit for the level populations. The model accounts for the relatively small effects of the time variation of the electron temperature and ionization processes. The rise of T_e is found to increase the $2p$ population by $25\pm5\%$, depending on the nature of the electron energy distribution (see Ref. 37 for more details). For the initial boron charge-state distribution (determined previously to be $50\pm20\%$ *B* II and $50\mp20\%$ *B* III), the increase of the *B* III density due to ionization processes is $20\pm10\%$. We note that for the modeling above we also estimated the effect of the *B* III flow during the current pulse on the observed *B* III level populations.

To estimate the variation of the boron density as a result of flow of the *B* III ions, we measured the velocities of *B* III along the x and z directions from Doppler shifts. We make a distinction here between the initial rise of the *B* III $2p$ population ($t<200$ ns) when the *B* III axial velocity is found to be $<3\times10^6$ cm/s and during the subsequent drop when the axial velocity rises to 8×10^6 cm/s. Integrating these velocities with respect to time the *B* III axial displacement is found to be ≈0.2 cm during the rise of the light intensities and another 0.3 cm during the 50 ns drop. The axial displacement is negligible since the doped boron cloud is ~2 cm wide.

The *B* III x-velocity, obtained from Doppler shifts in observations through a slot in the flashboard, is found to be ~1.5 times smaller than the axial velocity. Taking into account the initial distribution of *B* III and its gradient along the x direction, the x direction *B* III flow is estimated to lower the boron density between $t=120$ and 270 ns at $x=0.5$ by a factor of 2 while increasing the boron density at $x=1.8$ cm by 70% within the same time interval.

The time-dependent populations and the inferred $n_e(t)$ are given in Fig. 8. It can be seen that near the cathode the electron density rises from 3×10^{14} to 4.5×10^{14}, followed by a drop to $(1.1\pm0.4)\times10^{14}$ cm^{-3}. Near the anode, however, the variations of the electron density are smaller, i.e., n_e drops by a factor of two. The largest contribution to the error bar results from the uncertainty in the boron density change as a result of the boron flow.

Using data from different x and z positions in the A-K gap (at $y=0$) we constructed a 2D map of n_e at different times. In this map different x positions are obtained in a

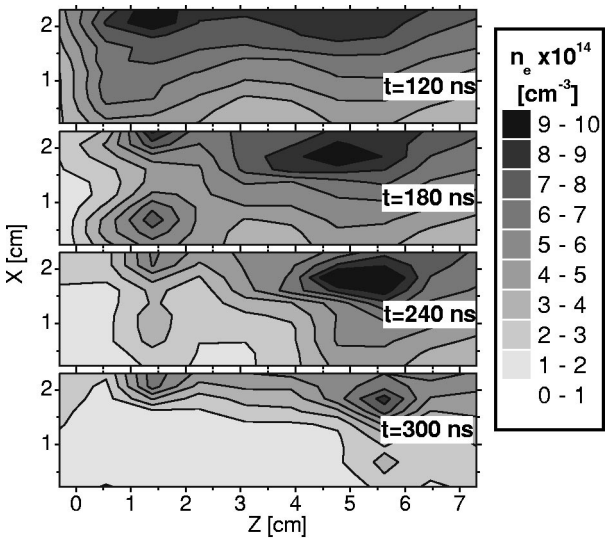

FIG. 9. Four 2D maps of the electron density in the center of the electrodes along the y direction obtained from the temporal evolution of the B III 2066 Å spectral line. The spatial resolutions are 0.45, 3, and 0.3 cm along the x, y, and z directions.

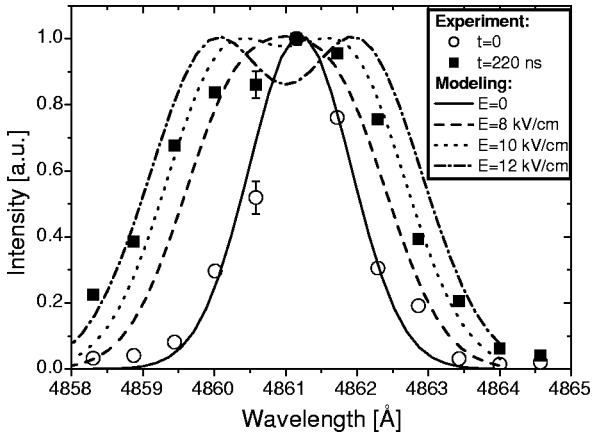

FIG. 10. Line profiles of the H_β line at $x=1$, $y=0$, and $z=3.7$ cm. The experimental results (symbols) are shown for two times, $t=0$ ns and $t=220$ ns. The lines are calculations with a 17 eV hydrogen temperature, the measured electron density, and different quasi-static electric field amplitudes.

single discharge using the open slit method. Figure 9 shows four such 2D maps of the electron density for $t=120$, 180, 240, and 300 ns. We note that the axially averaged electron density drops significantly at all x-positions. It should be emphasized that measurements beyond the plasma edge ($z=7-10$ cm) showed no significant rise in the electron density, verifying that the average electron density at $z<7$ cm does not drop due to plasma flow in the z direction beyond $z=7$ cm. Note that the drop in the electron density is most pronounced near the cathode where the final electron density is around 1×10^{14} cm^{-3}.

The results presented show that the electron density drops over the entire A-K gap by the time the current starts to flow to the load. Near the cathode the minimum electron density is $\approx1\times10^{14}$ cm^{-3} while near the anode the drop is less pronounced and at $t=300$ ns a density of $\approx4\times10^{14}$ cm^{-3} remains. The drop strongly suggests plasma flow through the highly transparent electrodes since no rise in the plasma density on the load-side edge of the plasma is seen. Note that the carbon velocity, $\sim10^7$ cm/s, is expected to lead to an insignificant axial displacement, while due to the smaller A-K gap a similar velocity towards the electrodes can result in a significant density drop.

Based on the magnetic field gradients (see the 2D maps in Fig. 5), it appears plausible that the plasma motion is towards the two electrodes. These gradients suggest that plasma at $x<1$ cm is mainly accelerated towards the cathode while that at $x>1$ cm is pushed towards the anode.

F. Electric fields

The presence of nonthermal electric fields that may give rise to anomalous collisionality is investigated using Stark broadening of hydrogen and helium lines. The width of H_β is found to rise and drop, similarly to the line intensity (the H_β reaches its peak width 20–30 ns after the peak light intensity). The H_β profiles at $t=0$ and 220 ns, obtained at $x=1$, $z=3.7$ cm and integrated along the y direction, are shown in Fig. 10.

The analysis of the hydrogen line widths is similar to the detailed description given in Ref. 47. The hydrogen Doppler width, required for the analysis of the H_β profile is obtained from the Doppler-dominated H_α profile, whose width remains constant throughout the pulse, indicating a nearly constant hydrogen temperature of 17 ± 2 eV. The H_β can be affected by electric fields at different frequencies. The lack of H_α broadening implies that there are no high-frequency fields,[48] allowing us to calculate the H_β Stark broadening under the influence of quasi-static fields. The H_β profile is calculated for different single-valued quasi-static electric fields (that represent the typical amplitude of nonthermal fields in the plasma) taking into account also the broadening of particle fields[49] (based on the known electron density) and the known Doppler profile. Comparison between the measured and the calculated H_β line profiles shows that at $t=220$ ns (the time when the peak electric field amplitude is obtained) the typical amplitude of turbulent electric fields in the plasma is 10 ± 2 kV/cm.

Similar measurements and analysis were performed using the He I $4d(^1D)-2p(^1P^0)$ (4922 Å) and the He I $3p(^1P^0)-2s(^1S)$ (5015 Å) lines. The 5015 Å line, which is insensitive to electric fields, broadens only slightly (from 0.2 to 0.25 Å FWHM), indicating that the influence of Doppler broadening remains small throughout the pulse. The 4922 Å line however, broadens from 0.5 Å at $t=0$ to 1.05 ± 0.1 Å at $t=220$ ns. Here too, the measured line profiles were compared to calculations[50] based on a nonthermal quasi-static electric field, the electron density determined in Sec. III E, and the Doppler width obtain from the 5015 Å line. For this line the non-negligible Zeeman splitting was also taken into account to yield an electric field amplitude of 10 ± 2 kV/cm.

We thus conclude that the electric field amplitude obtained from both the hydrogen and the helium line broadenings is $\sqrt{\langle E^2\rangle}=10\pm2$ kV/cm.

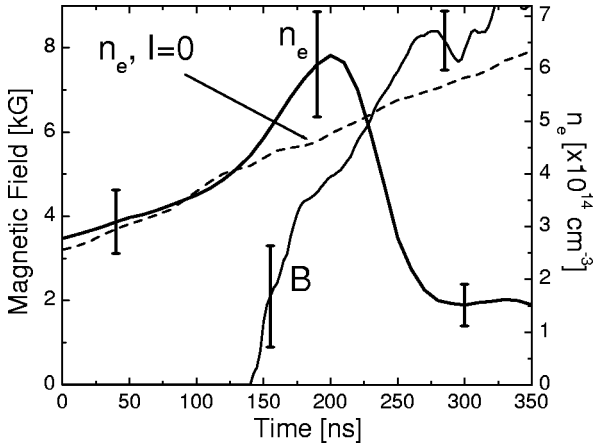

FIG. 11. The evolution of the magnetic field averaged over two discharges and the temporal behavior of the electron density as determined in Sec. III E. The results are at the center of the switch along the y direction, at $x=1$ cm, and $z=3.7$ cm. The dashed curve shows the electron density evolution without the application of the current pulse.

In a previous investigation of a coaxial 100 ns-duration plasma opening switch experiment we demonstrated[39] the presence of 14 kV/cm turbulent electric fields from Stark broadening of H_α and H_β. However, in that work, it was shown that most of these fields are high-frequency oscillations (Langmuir oscillations) $\omega_{ce}<\omega<\omega_{pe}$, where ω_{ce} is the electron cyclotron frequency and ω_{pe} is the electron plasma frequency. In the present study the narrowness of H_α suggests that the turbulent electric fields have a relatively low frequency ($\omega \leqslant \text{few}\times 10^{10}\ \text{s}^{-1}$).

IV. DISCUSSION

A. Correlation of the temporal variation of the magnetic field and electron density

In order to obtain a detailed understanding of the interaction between the magnetic field and the plasma detailed measurements of the ion dynamics are required. In a future publication[29] we will present such results and analyze them in the context of the recently demonstrated[22,28] simultaneous field penetration and plasma reflection, found to occur in multi-ion-species plasmas. Here, we wish to study the relation between magnetic field penetration and plasma flow based on the local magnetic field and electron density measurements. For this purpose, it is instructive to plot the observed magnetic field and electron density as a function of time for the same location, as given in Fig. 11 for the middle of the plasma. It is seen that while the magnetic field rises the electron density rises until the field reaches a value of ~ 5 kG, it then drops sharply as the magnetic field continues to rise to its peak value. This finding is seen for all positions with the density reaching its peak value at magnetic fields of 4–5.5 kG.

Let us analyze the various factors that may affect the electron density. First, the electron density may rise due to the continuous flow of the flashboard plasma. This effect is shown by the dashed line, which gives the rise in the electron density when no current pulse is applied. Another reason for the rise in the electron density is the ionization that occurs during the current pulse. Calculations based on the rise of the electron energy during the current pulse[37] show that at $t=200$ ns, ionization increases the electron density by only $10\pm 5\%$, bringing the electron density to the lowest-value edge of the error bar of the measured electron density. The additional rise of the electron density must thus result from plasma pushing, leading to an increased density within the current channel, consistent with the reflection of protons[28] and the predetermined proton density. On the other hand, the velocity of the heavier carbon ions, obtained from Doppler shifts,[28] shows a peak velocity that is 3 to 4 times smaller than that of the magnetic field, making their contribution to the electron density rise negligible.

At $t>200$ ns a substantial drop in the electron density (to a value 4 to 5 times smaller than that without the current pulse) is seen. Based on the analysis above, this drop is mainly caused by the expulsion of the proton plasma. The electron density that is expected to remain behind after the proton expulsion is $(3.5\pm 1)\times 10^{14}\ \text{cm}^{-3}$, which is more than two times higher than the measured electron density. We may thus conclude that pushing of the carbon plasma leads to an additional drop of the electron density to the observed density minimum of $(1.5\pm 0.5)\times 10^{14}\ \text{cm}^{-3}$. The carbon velocities show that the carbon ions are approximately motionless until $t=200$ ns, then attaining higher velocities that allow for a flow of ~ 1 cm up to $t=300$ ns, supporting the claim that the carbon–plasma motion is responsible for the density drop in the back of the current channel ($t>240$ ns in Fig. 11). Since this carbon–ion motion is much smaller than the axial plasma extent, a pure axial motion cannot explain the density drop that is observed at all axial positions. The A–K gap in our geometry is, however, comparable to the carbon-ion displacement, leading to the conclusion that the density drop probably results from the carbon–plasma motion towards and through the electrodes. Moreover, the density remaining at $t>300$ ns (about 1/2 of the initial carbon plasma density) can be attributed to carbon ions for which the motion is mainly axial, thus not contributing significantly to the density drop. We also note that the density of ions that are heavier[45] than carbon is much smaller than the electron density prevailing after $t\approx 300$ ns, so that they contribute negligibly to this density.

B. Circuit inductance

The measured space- and time-dependent magnetic field allows us to calculate the change in the circuit inductance during the plasma current conduction. The relation between the evolution of the magnetic field and the change in the inductance between $t=0$ and time t is expressed as

$$\Delta L(t)=\frac{\mu_0}{aB_G(t)}\int_0^d dx\int_{z_0}^{\infty} dz\, B(z,x,t), \tag{3}$$

where d is the A-K gap and we assume that the plasma boundary at the generator side does not move (justified by the low carbon velocities[29]).

In Sec. III C we showed that the magnetic field propagates in the z direction at a nearly constant velocity. More-

over, in Fig. 4 we showed that the measured 1D magnetic field distribution $B(z,t)$ can be fitted by Eq. (2) with $p=0.25$, $z_0=-2.2$ cm, $v=3.0\times10^7$ cm/s, $B_0=10$ kG, and $\tau=300$ ns. Inserting the magnetic field from Eq. (2) into Eq. (3) yields

$$\Delta L(t)=\frac{\mu_0 d}{a}\int_{z_0}^{vt+z_0}dz\left[1-\frac{(z-z_0)}{vt}\right]^p=\frac{\mu_0 dvt}{a(p+1)}, \quad (4)$$

which for our case yields a rate of inductance change of $dL/dt=43$ mH/s.

The change in the circuit inductance, associated with the propagation of the current channel, can also be obtained, as is commonly done, from the comparison of I_{plasma}, the upstream current in our experiment to I_{metal}, the upstream current in experiments with a metal plate positioned at the generator-side edge of the plasma. Since the upstream voltage for the two experiments is the same, one may express the inductance change by: $\Delta L(t)=L_0(I_{\text{metal}}-I_{\text{plasma}})/I_{\text{plasma}}$, where L_0 is the upstream inductance. This technique yields an inductance that increases approximately linearly in time reaching 12 ± 1.5 nH at $t=300$ ns, which corresponds to a mean rate of inductance change of 40 mH/s. Hence, to within the uncertainties, the inductance change derived from the upstream current measurements agrees with the simple 1D model, based on the detailed magnetic field measurements at $x=1$ cm.

C. Energy dissipation

The energy dissipation in the plasma due to the magnetic field penetration can be calculated from the measured magnetic field distribution. The amount of electromagnetic energy that flows into the entire plasma is found by integrating the Poynting flux at a plane normal to the electrodes at the generator-side edge of the plasma. The Poynting flux per unit width in the y direction at the plasma boundary at a time t is given by

$$P(z=z_0,t)=\frac{1}{\mu_0}V(z=z_0,t)B(z=z_0,t), \quad (5)$$

where the loop voltage is

$$V(z=z_0,t)=\frac{\partial}{\partial t}\int_0^d dx\int_{z_0}^{\infty}dz\,B(z,x,t). \quad (6)$$

The magnetic field is assumed to be uniform in the vacuum region between the two electrodes. Integrating the Poynting flux with respect to time yields the total energy that enters the plasma

$$U_{\text{in}}(z\geqslant z_0,t)=\int_0^t dt'\,P(z=z_0,t'). \quad (7)$$

The magnetic-field energy that is accumulated in the plasma is

$$U_B(z\geqslant z_0,t)=\int_0^d dx\int_{z_0}^{\infty}dz\,\frac{B^2(z,x,t)}{2\mu_0}. \quad (8)$$

The fraction of energy that is dissipated is then given by

$$\frac{U_{\text{in}}-U_B}{U_{\text{in}}}=1-\frac{\int_0^d dx\int_{z_0}^{\infty}dz\,B^2(z,x,t)}{2\int_0^t dt'\,B(z=z_0,t)\frac{\partial}{\partial t}\int_0^d dx\int_{z_0}^{\infty}dz\,B(z,x,t)}. \quad (9)$$

Assuming that the plasma edge, located at $z=z_0$ is motionless and using Eq. (2) for the magnetic field distribution, the magnetic field energy per unit width is

$$\begin{aligned}U_B&=\int_0^d dx\int_{z_0}^{\infty}dz\,\frac{B^2(z,x,t)}{2\mu_0}\\&=dvt\,\frac{B_0^2}{2\mu_0}\left(\frac{t}{\tau}\right)^2\int_0^1(1-\xi)^{2p}d\xi\\&=\frac{B_0^2}{2\mu_0}\left(\frac{t}{\tau}\right)^2\frac{dvt}{2p+1},\end{aligned} \quad (10)$$

where the energy that enters the plasma per unit width is

$$\begin{aligned}U_{\text{in}}&=\int_0^t dt'\frac{B(z=z_0,t')}{\mu_0}\frac{\partial}{\partial t'}\int_0^d dx\int_{z_0}^{\infty}dz\,B(z,x,t')\\&=\int_0^t dt'\left(\frac{B_0}{\mu_0}\frac{t'}{\tau}\right)\left(\frac{2B_0 dv}{(p+1)}\frac{t'}{\tau}\right)\\&=\frac{2}{3\mu_0}B_0^2\left(\frac{t}{\tau}\right)^2\frac{dvt}{p+1}.\end{aligned} \quad (11)$$

Hence, the fraction of dissipated energy is given by

$$\frac{U_{\text{in}}-U_B}{U_{\text{in}}}=1-\frac{3(p+1)}{4(2p+1)}. \quad (12)$$

Thus, in the limits described above, $p\to0$ (rectangular pulse) and $p\to1$ (a magnetic field linearly decreasing with z), the fractions of the dissipated magnetic field energy are 1/4 and 1/2, respectively. For the experimental value of $p=0.25$ the dissipation fraction is 0.375. Moreover, by multiplying this fraction by the time-integrated Poynting flux gives the dissipation in Joule/m

$$\begin{aligned}U_D(t)&=\left[1-\frac{3(p+1)}{4(2p+1)}\right]U_{\text{in}}(t)\\&=\frac{1}{3}\left[\frac{5p+1}{(2p+1)(p+1)}\right]\frac{B_G^2}{2\mu_0}dvt.\end{aligned} \quad (13)$$

The dissipated energy partitioning between the electrons and ions in the plasma will be discussed in subsequent publications.[29,37] Here, we only estimate the energy dissipation per electron (the electron density in the plasma is higher than the ion density), by dividing Eq. (13) by the number of electrons that initially reside in the volume penetrated by the magnetic field, i.e.,

$$U_{D,N}\cong\frac{U_D}{n_e dvt}=\frac{1}{3}\left[\frac{5p+1}{(2p+1)(p+1)}\right]\frac{B_G^2}{2\mu_0 n_e}, \quad (14)$$

which yields, for our conditions, a dissipation $U_{D,N}\cong0.4(B_G^2/2\mu_0 n_e)$ that at $t=300$ ns amounts to ≈2.0 keV per electron. The dissipation in the case of a linear rise-in-time of the current is, therefore, significantly smaller than in the

case of a step function rise-in-time of the current, for which the dissipation is $U_{D,N}=B_G^2/2\mu_0 n_e$. Moreover, the exact value of the dissipation depends on the magnetic field profile, demonstrating again the importance of accurate knowledge of the magnetic field spatial distribution.

D. Mechanism of magnetic field penetration

Here we discuss the mechanism of magnetic field penetration into the plasma. It is natural to examine the possibility that the fast penetration of the magnetic field is a result of a high anomalous resistivity. That high resistivity would result in a high inductive electric field of the form

$$\vec{E}=\eta_{\mathrm{an}}\,\vec{j}. \tag{15}$$

As is clearly seen in Fig. 4, the intensity of the magnetic field is decreasing axially in the direction of the load. Assuming that the inductive electric field that causes the magnetic field penetration is mostly perpendicular to the electrodes (along the x direction), it, too, should decrease axially towards the load. However, as can also be inferred from Fig. 4, the current density is rather increasing axially. Therefore, in order to obtain an electric field that decreases in the z direction, the anomalous resistivity should strongly decrease axially towards the load, being smallest at the magnetic field front, where the current density peaks. Since, however, the high current density is expected to be the source of the anomalous resistivity, it does not seem reasonable that the resistivity be smallest there. Thus, the profile of the magnetic field with a high current density at the front indicates that an anomalously high resistivity is not the source of the fast magnetic field penetration.

The indication that an anomalously high resistivity is not the source of the fast magnetic field penetration can be further supported by comparing the estimated anomalous collisionality to the collisionality required for diffusion at the observed magnetic-field propagation velocity. The required diffusion rate can be estimated using the plasma axial extent $l\approx 10$ cm and the magnetic field penetration time $t\approx 380$ ns to be $D=l^2/t\approx 2.6\times 10^8$ cm^2/s. The associated electron collision frequency is $\nu_{ei}\approx 3\times 10^{11}$ s^{-1}, which is approximately $2\omega_{ce}$ at the maximum magnetic field. Let us estimate the anomalous collisionality that results from some current-driven instabilities.

The instability that can result in the highest collision frequency, the ion-acoustic instability, has been investigated[11,38,39] in different configurations. Let us estimate the anomalous plasma collision frequency using the measured nonthermal electric field amplitude (as described in Sec. III F). The effective collision frequency ν_{ei}^{iac}, resulting from the ion–acoustic instability, is approximately[38,39]

$$\nu_{ei}^{iac}\cong\omega_{pe}\frac{\varepsilon_0\langle E^2\rangle}{2n_eT_e}, \tag{16}$$

where E is the amplitude of the instability electric fields and ε_0 is the permittivity of free space. Using the observed amplitude of the turbulent electric field, 10 ± 2 kV/cm, and taking a lower bound on $T_e=10$ eV, we obtain an upper bound $\nu_{ei}^{iac}<6\times 10^9$ s^{-1} for the ion–acoustic collisionality. Although this collisionality is a couple of times larger than the Spitzer collisionality[16] ($\nu_{\mathrm{spitzer}}\sim 10^9$ s^{-1}), the resulting diffusion coefficient is still fifty times smaller than required for explaining the magnetic field propagation in terms of diffusion.

While the Buneman instability is not expected to grow since the electron drift velocity is not higher than the electron thermal velocity, the lower-hybrid drift instability[2] may become unstable in our configuration. Following the nonlinear mode coupling analysis of Drake *et al.*,[51] the anomalous collision frequency can be expressed as $\nu_{ei}^{\mathrm{lh}}\cong 2.4(V_{\mathrm{di}}/v_i)^2\omega_{\mathrm{lh}}$, where ω_{lh} is the lower hybrid frequency, v_i is the ion thermal velocity, $V_{\mathrm{di}}=v_i(r_{Li}/2L)$ is the ion diamagnetic drift velocity, and r_{Li} is the ion Larmor radius. For our experimental parameters $(V_{\mathrm{di}}/v_i)\sim 1/3$, resulting in an anomalous collision frequency $\nu_{ei}^{\mathrm{lh}}\approx 5\times 10^8$ s^{-1} that is ten times smaller than the collisionality estimated above to result from the ion acoustic instability.

Therefore, both the axial profile of the magnetic field and the above estimates of the anomalous resistivity suggest that an enhanced electric field of the form given by Eq. (18) is not expected to cause the penetration. However, an axial electric field that is stronger inside the current channel, as is the case for the Hall electric field, could explain the fast magnetic field propagation. A Hall electric field that varies along the x direction due to plasma nonuniformities together with a small but finite resistivity has been shown to cause a fast penetration of the magnetic field.[14] However, a quantitative estimate of the magnetic field penetration due to the Hall field,[20] for the measured initial electron-density gradient in the x direction[45] in this experiment, yields a velocity of 2×10^7 cm/s, significantly lower than the measured velocity of the magnetic field propagation. Furthermore, as described in Sec. III D, the penetration appears to be independent of the relative directions of the current and the density gradient, which contradicts the expected evolution due to Hall-field mechanism. The measured current-channel width is also inconsistent with an evolution that is dominated by the Hall-field mechanism in an initially nonuniform plasma[43] that should result in a current channel width of $(c/\omega_{pe})^2\nu_{ei}/v$. For our experimental parameters and the above-calculated collisionality of the ion acoustic instability the current-channel width should be only 0.18 cm, approximately ten times less than the measured width. It seems therefore that the magnetic field penetration into the plasma is not caused by the Hall mechanism due to the initial density gradient across the A-K gap.

We explore here the possibility that an inductive Hall electric field that results from small-scale (smaller than our spatial resolution of a few mm) density fluctuations generated by instabilities causes the fast penetration. If indeed turbulence that leads to the formation of density fluctuations exists in the plasma, it could enhance the rate at which the Hall mechanism allows penetration, by reducing the space scale L in the expression of the Hall velocity. Moreover, such a mechanism should be independent of the current flow direction, consistent with the findings described in Sec. III D. Since the Hall mechanism can lead to field penetration only in regions where the density decreases along the current flow,

we should expect elongated finger-like structures to form. Rapid diffusion, due to the small scale of the gradients, is expected to lead to field penetration into the entire plasma volume. The observed magnetic field penetration and the broad current-channel width could then be attributed to spatial integration over the finger-like structure. Magnetic field penetration due to the Hall field in the presence of small-scale density nonuniformities has been suggested in the past.[19,40,41] It could be related to magnetic field reconnection that is enhanced by the Hall fields as has been recently suggested[52,53] It may also be related to complex magnetic field structures that have been observed in a θ-pinch[13] using magnetic probes, and were associated with a tearing instability.

We suggest that the unmagnetized Rayleigh–Taylor instability[42,54] (or large Larmor radius Rayleigh–Taylor instability) that can occur in sub-Alfvénic plasma expansions[55,56] could be responsible for the above mentioned density fluctuations. This instability is driven by an acceleration of an inhomogeneous plasma ($\nabla n_e \neq 0$). The effective acceleration (in analogy to the gravitational acceleration) is given by $g=-dv_i/dt$ so that the instability can occur when $g\cdot\nabla n_e<0$. This situation occurs at the plasma boundary where $dn_e/dz>0$ and the effective gravity, associated with the proton acceleration is negative. Although this instability has the same driving mechanism as the conventional Rayleigh–Taylor instability ($g\cdot\nabla n_e<0$), it has very different linear and nonlinear behaviors. The linear growth rate of the instability is $\gamma=k_x\sqrt{gL}$, where k_x is the wave number perpendicular to the density gradient and L is the scale length of the density gradient at the plasma boundary. The expression for the linear growth rate applies for $g/L>\omega_{ci}^2/4$, where ω_{ci}^2 is the ion cyclotron frequency, i.e., the ions are unmagnetized. The instability is compressible $\nabla\cdot v_i\neq 0$ and has $\nabla\times v_i=0$, which is opposite the conventional Rayleigh–Taylor instability. Thus, as has been shown,[57] rather than corrugating the surface of the magnetic field-plasma interface, the instability lead to ion lumping.

We can estimate the parameters g, L, ω_{ci}, and γ for our experiment as follows. Based on the magnetic field profile (see Fig. 4) we estimate[28] it takes at most $\Delta t\sim 60$ ns for the protons to accelerate to a velocity that is twice the magnetic field velocity; $v_p\sim 6\times 10^7$ cm/s. This yields a lower bound for the effective acceleration $g\sim 10^{15}$ cm/s^2. We take $B\sim 5$ kG, the value of the magnetic field when the electron density starts to drop (see Fig. 11) so that $\omega_{\mathrm{ci}}\sim 5\times 10^7$ s^{-1} for protons and estimate $L\sim 1$ cm. For these numbers one finds that $g/L\sim 10^{15}$ and $\omega_{ci}^2/4\sim 6\times 10^{14}$ so that the turn-on condition of the unmagnetized Rayleigh–Taylor instability is satisfied (in fact, the mean proton cyclotron frequency is smaller since it is estimated that the proton reflection occurs at $B\sim 5$ kG, reducing the mean ω_{ci}).

The spatial scale of such possibly-formed fluctuations is not known, however, being not observable by our present measurements spatial resolution, their scale must be less than a few mm. Assuming that the fluctuation scale length should be at least several times the electron skin depth (which is ≈ 0.3 mm in our plasma), we choose a reasonable wavelength $\lambda\approx 0.1$ cm. For this wavelength and a modulation of, say $\sim 15\%$ of the proton density, the Hall velocity is consistent with the measured magnetic field velocity. To estimate the growth rate we use $k_x=2\pi/\lambda\sim 62$ cm^{-1} and find that $\gamma\sim 6.2\times 10^8$ s^{-1}, so that the e-folding time is $\tau\sim 1.6$ ns, which is sufficiently rapid to allow the instability to grow before the magnetic field propagates a significant distance.

Hence, if this instability grows in our experiment, and if $\lambda\approx 0.1$ cm and the density variations in the formed finger-like structures is on the order of $\pm 0.3\times 10^{14}$ cm^{-3}, the magnetic field is expected to penetrate at a Hall velocity that for $B=5$ kG is 3×10^7 cm/s, consistent with the observed velocity.

Note that because of the dependence of the Hall penetration on the direction of the density gradients in the plasma, the Hall effect may not lead to field penetration into the entire structures here discussed. Thus, while the spatially fluctuating density gradients are expected to cause field penetration into parts of the density structures through the Hall mechanism, other parts may still remain unpenetrated by the field. However, for spatial scales of ~ 1 mm, even Spitzer resistivity is estimated to be sufficiently high to lead to the completion of the field penetration into the entire plasma.

We have, in fact, indirect indications to the presence of small-scale magnetic field nonuniformities. As will be described in a future publication, polarization-dependent measurements of the magnetic field along different directions indicate the presence of magnetic field components other than B_y, indicating current flow also in the y direction. The amplitude of these magnetic field components is sufficiently small to assure that the correction to the total magnetic field is smaller than the indicated errors of the magnetic field. We note that if small-scale finger-like structures form, the presented magnetic-field amplitude describes the spatially averaged magnetic field.

Furthermore, the broad axial-velocity distributions of the ions observed in the entire plasma[29] imply that in regions of comparable size to the observation spatial resolution (~ 5 mm), different ions are accelerated in different directions, presumably as a result of structure in the accelerating magnetic field. As described in Sec. III E the density that remains at $x<1.5$ cm and $z<5$ cm at $t=300$ ns is much higher than expected from the known heavy-ion densities, suggesting that not all carbon ions are significantly pushed by the magnetic field piston. In our experimental configuration, the main pushing of the plasma that leads to the observed density drop is due to acceleration towards the electrodes since the plasma x dimension is much smaller than the plasma length (in the z direction). The assumption of finger-like magnetic field structures may explain this finding since such structures are expected to lead to ion acceleration also axially, preventing part of the ions from moving out across the A-K gap. The continued presence of plasma behind the magnetic piston may explain the low switch impedance during its opening, observed in numerous[58,59] long-conduction POSs.

V. SUMMARY

Time and space resolved measurements of the magnetic field from Zeeman splitting, the electron density from line intensities, and the amplitude of turbulent electric fields from Stark broadening are presented. The magnetic field is found to rapidly penetrate into the plasma. The measured magnetic field is used to estimate the expected dissipation in the plasma and the change in the circuit inductance, associated with the propagating magnetic field.

The magnetic field profile indicates that the field penetration is not due to diffusion processes. Moreover, based on the measured turbulent electric fields it appears that the ion–acoustic and lower-hybrid drift instabilities do not provide a sufficiently high resistivity to cause fast enough field diffusion. On the other hand, the observed insensitivity of the field penetration on the current flow direction contradicts an explanation based on the Hall-field mechanism and on the initial average electron density gradient across the A-K gap. We thus propose an alternative explanation for the magnetic field penetration into the plasma, based on the formation of small-scale spatial density fluctuations. These fluctuations provide relatively large density gradients that enhance the penetration due to the Hall field. Furthermore, due to the fluctuating gradient directions, the penetration becomes insensitive to the polarity of the current generator. The unmagnetized Rayleigh–Taylor instability, associated with the acceleration of the protons by the magnetic field, is suggested as a possible source for the small-scale density fluctuations; however, the possibility that such density fluctuations are produced by other instabilities should also be investigated.

The results of the present investigations demonstrate the need for detailed measurements of the properties of the plasma and the electromagnetic fields in order to elucidate the complicated phenomena that dominate the conduction of rapidly rising currents in plasmas. It appears that future measurements require high spatial resolution in order to develop models for possible onset of magnetohydrodynamic turbulence and its implications on the magnetic field evolution. We believe that this work should encourage the development of theoretical models to address the detailed behavior of multispecies plasmas that exhibit simultaneous pushing and magnetic field penetration.

ACKNOWLEDGMENTS

The authors wish to thank Yu. V. Ralchenko and E. Stambulchik for their aid in the atomic-physics calculations and G. Baruch for his help in computations. We are indebted to A. Fisher, Y. Krasik, J. F. Drake, and A. Weingarten for fruitful discussions and P. Meiri for his skilled technical assistance.

This work was supported by United States–Israel Binational Science Foundation and by the German–Israeli Project Cooperation Foundation (DIP).

[1] J. Wesson and D. J. Campbell, *Tokamaks* (Oxford University Press, Oxford, 1997).
[2] R. J. Commisso and H. R. Griem, Phys. Fluids **20**, 44 (1977).
[3] P. Bogen and E. Hintz, ''Shock induced plasmas,'' in *Gaseous Electronics*, edited by M. N. Hirsch and H. J. Oskam (Academic, New York, 1978), Vol. 1, p. 453.
[4] T. A. Mehlhorn, IEEE Trans. Plasma Sci. **25**, 1336 (1997), and references therein.
[5] See, for example, ''Special issue on plasma opening switches,'' IEEE Trans. Plasma Sci. **PS-15**, (1987), and references therein.
[6] W. Peter, A. Ron, and N. Rostoker, Phys. Fluids **26**, 2276 (1983).
[7] S. B. Mende, G. R. Swenson, S. P. Geller, J. H. Doolittle, G. Haerendel, A. Valenzuela, and O. H. Bauer, J. Geophys. Res. **94**, 17063 (1989).
[8] M. J. Aschwanden, A. I. Poland, and D. M. Rabin, Annu. Rev. Astron. Astrophys. **39**, 175 (2001).
[9] K. J. H. Phillips, Plasma Phys. Controlled Fusion **42**, 113 (2000).
[10] C. Litwin, R. Rosner, and D. Q. Lamb, Mon. Not. R. Astron. Soc. **310**, 324 (1999).
[11] R. M. Kulsrud, R. F. Ottinger, and J. M. Grossmann, Phys. Fluids **31**, 1741 (1988).
[12] G. I. Dolgachev, L. P. Zakatov, Yu. G. Kalinin, A. S. Kingsep, M. S. Nitishinskii, and A. G. Ushakov, Fiz. Plazmy **22**, 1017 (1996).
[13] J. H. Irby, J. F. Drake, and H. R. Griem, Phys. Rev. Lett. **42**, 228 (1979).
[14] R. Shpitalnik, A. Weingarten, K. Gomberoff, Ya. Krasik, and Y. Maron, Phys. Plasmas **5**, 792 (1998).
[15] J. D. Huba, J. M. Grossmann, and P. F. Ottinger, Phys. Plasmas **1**, 3444 (1994).
[16] N. A. Krall and A. W. Travelpiece, *Principles of Plasma Physics* (McGraw–Hill, New York, 1973).
[17] M. Rosenbluth, *Plasma Physics and Thermonuclear Research*, edited by C. L. Longmire, J. T. Tuck and W. B. Thompson (Pergamon, London, 1963), p. 271.
[18] A. S. Kingsep, Yu. V. Mohkov, and K. V. Chukbar, Sov. J. Plasma Phys. **10**, 495 (1984).
[19] A. V. Gordeev, A. S. Kingsep, and L. I. Rudakov, Phys. Rep. **243**, 215 (1994).
[20] A. Fruchtman, Phys. Fluids B **3**, 1908 (1991).
[21] M. Sarfaty, Y. Maron, Ya. E. Krasik, A. Weingarten, R. Arad, R. Shpitalnik, A. Fruchtman, and S. Alexiou, Phys. Plasmas **2**, 2122 (1995).
[22] A. Weingarten, R. Arad, A. Fruchtman, and Y. Maron, Phys. Rev. Lett. **87**, 115004 (2001).
[23] L. I. Rudakov, Phys. Plasmas **2**, 2940 (1995).
[24] G. G. Spanjers, E. J. Yadlowsky, R. C. Hazelton, and J. J. Moschella, J. Appl. Phys. **77**, 3657 (1995).
[25] R. J. Commisso, R. A. Riley, J. M. Grossmann, B. V. Weber, D. D. Hishelwood, T. G. Jones, P. F. Ottinger, S. B. Swanekamp, and J. J. Watrous, *Proceedings of the XII International Conference on High-Power Particle Beams*, Haifa, 1998, edited by M. Markovits and J. Shiloh (IEEE, Piscataway, NJ, 1999), Vol. 1, p. 265.
[26] R. Arad, K. Tsigutkin, Yu. V. Ralchenko, A. Fruchtman, N. Chakrabarti, and Y. Maron, in Ref. 25, p. 253.
[27] A. Chuvatin and B. Etlicher, Phys. Rev. Lett. **74**, 2965 (1995).
[28] R. Arad, Ph.D. thesis, Weizmann Institute of Science, Rehovot, Israel (2002); K. Tsigutkin, R. Arad, A. Fisher, and Y. Maron, *Proceedings of the 13th International Conference on High-Power Particle Beams*, Nagaoka, 2000 (Nagaoka University of Technology, Nagaoka, 2001), p. 111.
[29] R. Arad, K. Tsigutkin, A. Fruchtman, and Y. Maron, ''Investigation of the ion dynamics in a multi-ion-species plasma under pulsed magnetic fields,'' Phys. Plasmas (to be submitted).
[30] D. D. Hinshelwood, J. R. Boller, R. J. Commisso, G. Cooperstein, R. A. Meger, J. M. Neri, P. F. Ottinger, and B. V. Weber, Appl. Phys. Lett. **49**, 1635 (1986).
[31] R. J. Commisso, P. J. Goodrich, J. M. Grossmann, D. D. Hinshelwood, P. F. Ottinger, and B. V. Weber, Phys. Fluids B **4**, 2368 (1992).
[32] V. M. Bystritskii, Ya. E. Krasik, I. V. Lisitsyn, and A. A. Sinebrykhov, IEEE Trans. Plasma Sci. **19**, 607 (1991).
[33] B. V. Weber and D. D. Hinshelwood, Rev. Sci. Instrum. **63**, 5199 (1992); B. V. Weber and S. F. Fulghum, *ibid.* **68**, 1227 (1997).
[34] D. Hinshelwood, B. Weber, J. M. Grossmann, and R. J. Commisso, Phys. Rev. Lett. **68**, 3567 (1992).
[35] R. Arad, L. Ding, and Y. Maron, Rev. Sci. Instrum. **69**, 1529 (1998).
[36] B. V. Weber (private communication, 1998).
[37] R. Arad, Yu. V. Ralchenko, and Y. Maron, ''Observation of non-Maxwellian electron energy distribution in a current carrying plasma,'' Phys. Rev. E (to be submitted).
[38] A. S. Kingsep, Sov. J. Plasma Phys. **17**, 342 (1991).
[39] A. Weingarten, S. Alexiou, Y. Maron, M. Sarfaty, Ya. Krasik, and A. S. Kingsep, Phys. Rev. E **59**, 1096 (1999).

[40]A. S. Kingsep, K. V. Chukbar, and V. V. Yan'kov, *Reviews of Plasma Physics*, edited by B. B. Kadomtsev (Consultants Bureau, New York, 1990), Vol. 16.
[41]A. Fruchtman and L. I. Rudakov, Phys. Rev. Lett. **69**, 2070 (1992).
[42]A. B. Hassam and J. D. Huba, Geophys. Res. Lett. **14**, 60 (1987).
[43]A. Fruchtman, Phys. Rev. A **45**, 3938 (1992).
[44]A. Fruchtman, A. A. Ivanov, and A. S. Kingsep, Phys. Plasmas **5**, 1133 (1998).
[45]R. Arad, K. Tsigutkin, Yu. V. Ralchenko, and Y. Maron, Phys. Plasmas **7**, 3797 (2000).
[46]M. E. Foord, Y. Maron, and E. Sarid, J. Appl. Phys. **68**, 5016 (1990).
[47]E. Sarid, Y. Maron, and L. Troyansky, Phys. Rev. E **48**, 1364 (1993).
[48]D. H. Oza, R. L. Greene, and D. E. Kelleher, Phys. Rev. A **38**, 2544 (1988).
[49]H. R. Griem, *Plasma Spectroscopy* (McGraw-Hill, New York, 1964); *Spectral Line Broadening by Plasmas* (Academic, New York, 1974).
[50]E. Stambulchik and Y. Maron, Phys. Rev. A **56**, 2713 (1997).
[51]J. F. Drake, P. N. Guzar, A. B. Hassam, and J. D. Huba, Phys. Fluids **27**, 1148 (1984); J. F. Drake (private communication, 2002).
[52]J. D. Huba and L. I. Rudakov, "Three-dimensional Hall magnetic reconnection," Phys. Rev. Lett. (submitted).
[53]L. I. Rudakov and J. D. Huba, Phys. Rev. Lett. **89**, 095002 (2002).
[54]J. D. Huba, A. B. Hassam, and D. Winske, Phys. Fluids B **2**, 1676 (1990); J. D. Huba, P. A. Bernhardt, and J. G. Lyon, J. Geophys. Res. **97**, 11 (1992); J. D. Huba, Phys. Plasmas **2**, 2504 (1995).
[55]P. A. Bernhardt, R. A. Roussel-Dupre, M. B. Pongratz, G. Haerendel, A. Valenzuela, D. Gurnett, and R. R. Anderson, J. Geophys. Res. **92**, 5777 (1987).
[56]B. H. Ripin, E. A. McLean, C. K. Manka, C. Pawley, J. A. Stamper, T. A. Peyser, A. N. Mostovych, J. Grun, A. B. Hassam, and J. D. Huba, Phys. Rev. Lett. **59**, 2299 (1987).
[57]J. D. Huba, J. G. Lyon, and A. B. Hassam, Phys. Rev. Lett. **59**, 2971 (1987).
[58]J. M. Grossmann, S. B. Swanekamp, P. F. Ottinger, R. J. Commisso, D. D. Hinshelwood, and B. V. Weber, Phys. Plasmas **2**, 299 (1995).
[59]J. R. Thompson (private communication, 2000).